Received: 18 July 2019 | Revised: 17 September 2019 | Accepted: 20 September 2019

DOI: 10.1002/aoc.5359

FULL PAPER

Applied Organometallic Chemistry WILEY

Copper-based Schiff Base Complex Immobilized on Core-shell Fe_3O_4@SiO_2 as a magnetically recyclable and highly efficient nanocatalyst for green synthesis of 2-amino-4*H*-chromene derivatives

Hakimeh Ebrahimiasl | **Davood Azarifar**

Department of Chemistry, Bu-Ali Sina University, Hamedan, 65178, Iran

Correspondence
Davood Azarifar, Department of Chemistry, Bu-Ali Sina University, Zip Code 65178, Hamedan, Iran.
Email: azarifar@basu.ac.ir

Funding information
Research Council of Bu-Ali Sina University

Abstract

Fe_3O_4-supported copper (II) Schiff-Base complex has been synthesized through post-modification with 1,3-phenylenediamine followed by further post-modification with salicylaldehyde and coordination with Cu(II) ion. The resulted Fe_3O_4@SiO_2-imine/phenoxy-Cu(II) magnetic nanoparticles (MNPs) were characterized by various techniques including SEM, TEM, XRD, XPS, EDX, VSM, FT-IR, and ICP. The catalytic activity as a magnetically recyclable heterogeneous catalyst for one-pot, three-component synthesis of 2-amino-4*H*-chromene derivatives was examined. The catalyst is efficient in the reaction and can be recovered by magnetic separation and recycled several times without significant loss in the catalytic activity.

KEYWORDS

2-amino-4*H*-chromene, Fe_3O_4-immobilized-Cu (II) Schiff-Base complex, magnetic nanoparticles, nanocatalyst, three-component reaction

1 | INTRODUCTION

In the last few decades, scientists have greatly concerned about the environmental health issues originating from catalytic processes and have made considerable efforts for development of eco-friendly recyclable catalysts for organic transformations such as multi-component reactions (MCRs) in the synthetic and industrial fields.[1–6] In recent years, immobilization of different homogeneous catalysts onto various nanoparticles has emmerged as a promising strategy for improving the catalytic efficiency and stability.[7] The last few decades have witnessed a considerable progress in the development of various magnetic nanoparticles (MNPs) as sustainable and efficient supports or catalysts in organic synthesis and industrial fields due to their interesting physical and chemical characteristics such as large surface to volume ratio, high atom efficiency, easy magnetic separation and high potential of recyclability.[8–13] As previously reported, the use of various magnetic metal oxides and hybrid metal oxide nanoparticles such as Fe_2O_3, Fe_3O_4, TiO_2, Al_2O_3, ZnO, and $La_{0.7}Sr_{0.3}MnO_3$ have attracted a massive attention both in industry and organic reactions as catalysts and/or supports.[14,15] Magnetic Fe_3O_4 nanoparticles have emerged as a privileged support for immobilization of various ligands and functional groups such as phosphorous, nitrogen and organic moieties owing to the presence of high density hydroxyl groups on their surface, high surface area, high stability, facile magnetic separation, environmental benignity and high loading capacity.[13,16–25] Among different nitrogen-based ligands, Schiff-Base ligands supported on magnetic nanoparticles immobilize in excellent state through the coordination to a variety of transition metals with improved catalytic activity and stability.[26–31] This is because the ligands containing *N*-donors exhibit a high performance by a

 © 2019 John Wiley & Sons, Ltd.

stable hosting a range of metal cations and as a result, these materials become excellent candidates in catalysis design as well as analytical, industrial and medicinal applications.[32–36] In comparison, the Cu-based catalysts have offered excellent alternatives to other noble-metal-based catalysts due to their interesting features including low price, facile separation and high catalytic performance.[37–39]In addition, another environmentally important synthetic approach is the use of multi-component reactions (MCRs) that have attracted enormous interest as convergent and high atom-economy processes.2f, h, 41–46

Among the heterocyclic compounds, chromenes and their derivatives are well-documented compounds of important biological and pharmacological importance which perform anticancer, spasmolytic, diuretic, anti-HIV, antimalarial, and anti-anaphylactic activities.[31,46–50] A large group of chromenes have been widely used as therapeutically useful agents such as acenocoumarol which functions as an anticoagulant and is used for the treatment of bronchial asthma.[51] Also, a wide variety of chromenes are naturally occurring products contained in many secondary metabolites, as pigments, flavonoids, and anthocyanin.[52,53] In addition, a variety of chromenes have found wide applications as pigments, cosmetics, and biodegradable agrochemicals.[54] The methods reported in the literatures for the synthesis of chromenes utilize various catalytic systems such as ionic liquids,[54] hexadecyltrimethyl ammonium bromide,[55] diammonium hydrogen phosphate (DAHP),[56] Mg/La mixed metal oxides,[57] α-Fe_2O_3 nanoparticles,[58] silica-grafted ionic liquid,[59] and $H_6P_2W_{18}O_{62}.18H_2O$.[60]

2 | EXPERIMENTAL

2.1 | General

Chemicals were purchased from Merck Chemical Company and used without further purification. Melting points were determined in open capillary tubes using a BUCHI 510 apparatus. Fourier transform infrared (FT-IR) spectra were recorded from KBr pellets on a Perkin Elmer GX FT-IR spectrometer. ^{1}H NMR and ^{13}C NMR spectra were recorded for samples in $CDCl_3$ or DMSO-d_6 on 90, 250 and 400 MHz BRUKER AVANCE instruments at ambient temperature using tetramethylsilane (TMS) as internal standard. Scanning electron microscopy (SEM) images were obtained on EM3200 instrument operated at 30 kV accelerating voltage. Energy-dispersive X-ray (EDX) analysis was carried out using a FESEM-SIGM (German) instrument. Thermo-gravimetric analysis (TGA) was recorded in air using TGA/DTA PYRIS DIAMOND instrument. Magnetic measurement of the catalyst was performed using a vibrating sample magnetometer (VSM) instrument MDKFT. Moreover, high resolution transmission electron microscopy (TEM) was conducted on the nanoparticles using a HRTEM Philips CM30, (300KV) instrument. Inductively coupled plasma optical emission spectroscopy (ICP-OES) was performed by Arcos EOP, 32 Linear CCD simultaneous ICP analyzer. X-ray photoelectron spectral (XPS) analysis was performed using a K-Alpha spectrometer. To gain an accurate understanding of the molecular structures of 2-amino-4*H*-chromene derivatives, geometry optimization and conformational analysis were performed in the gas phase with the Gaussian 09 suite of programs and the Beck's three-parameter hybrid method B3LYP with the 6-31G (d,p) basis set. Vibrational frequency analysis was also performed at the same level to ensure the structures are local minima. The natural bond orbital (NBO) method on the wave functions was obtained at the same level of theory by NBO 3.1 program.[61–64] The characterization data for the catalyst and the titled products are available online in the supporting information section at the end of the article (Scheme 1).

2.2 | Preparation of Fe_3O_4-supported copper (II) Schiff-base complex, Fe_3O_4@SiO_2-imine/phenoxy-Cu(II) (MNPs)

The Fe_3O_4@SiO_2-imine/phenoxy-Cu(II) core-shell magnetic nanoparticles were successfully prepared in six steps as depicted in Scheme 2 and explained bellow.

2.2.1 | Synthesis of SiO_2-modified core-shell Fe_3O_4 MNPs

Fe_3O_4 magnetic nanoparticles were synthesized by co-precipitation of Fe^{3+} and Fe^{2+} ions with $[Fe^{3+}]/[Fe^{2+}]$ molar ratio of 2:1 as described in the literature.[65] Shortly, $FeCl_3.6H_2O$ (5.4 g, 0.02 mol) and $FeCl_2.4H_2O$ (2.0 g, 0.01 mol) were dissolved in deionized water (80 ml) under nitrogen atmosphere with vigorous stirring. Then, 25% aqueous NH_4OH solution (10 ml) was added dropwise at the constant rate of 1 ml per min to the mixture at 80 °C in N_2 atmosphere that resulted in the formation of uniform black Fe_3O_4 magnetic nanoparticles. Then, these black particles were cooled to room temperature, washed twice with deionized water and 0.02 M aqueous NaCl solution consecutively, and decanted using an external magnet. In the following step, the as-prepared Fe_3O_4 nanoparticles (1 g) were dispersed

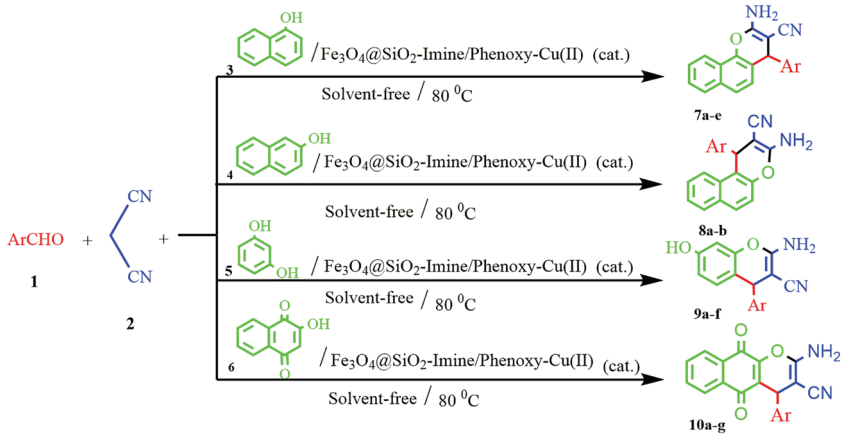

SCHEME 1 Three-component synthesis of various 2-amino-4*H*-chromene-3-carbonitrile derivatives catalyzed by Fe_3O_4@SiO_2-imine/phenoxy-Cu(II) MNPs

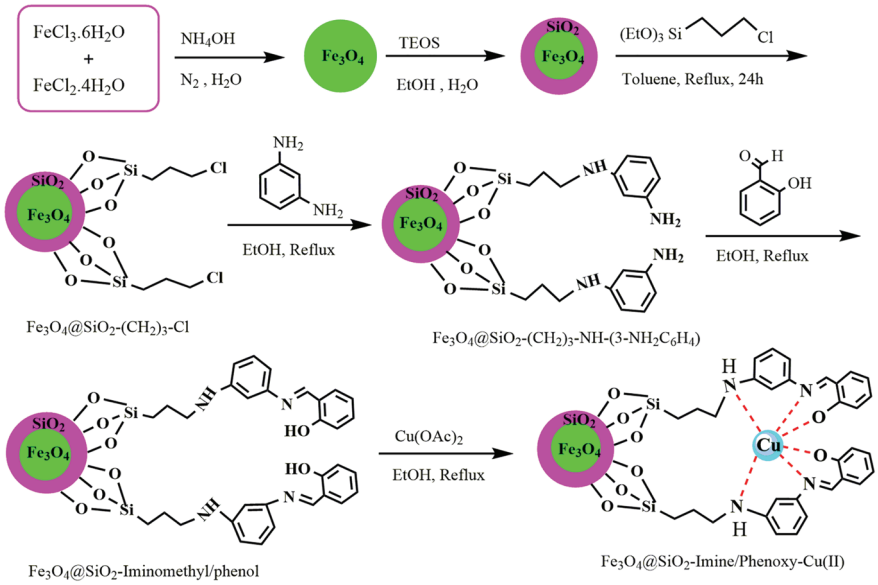

SCHEME 2 Stepwise preparation of Fe_3O_4@SiO_2-Imine/Phenoxy-Cu(II) MNPs

in a mixture of ethanol (100 ml) and deionized water (10 ml) containing 25% ammonia solution (2.5 ml). Then, tetraethyl orthosilicate (TEOS) (2 ml) was added dropwise and the stirring was continued for 2 hr at 60 °C. The resulted product was magnetically separated, washed repeatedly with deionized water and ethanol, and then dried in air for 4 hr.[66]

2.2.2 | Chloro-functionalization of Fe_3O_4–SiO_2

The prepared core-shell Fe_3O_4@SiO_2 (1 g) was added to a solution of (3-chloropropyl)triethoxysilane (CPTES) (3 ml) in dry toluene (100 ml) followed by stirring at 90 °C for 12 hr in N_2 atmosphere. Finally, chloropropyl-bonded magnetic nanoparticles (Fe_3O_4@SiO_2-$(CH_2)_3$-Cl) at the end of the reaction were repeatedly washed with toluene, separated by using a magnet and dried under reduced pressure.

2.2.3 | Immobilization of 1,3-phenylenediamine on Fe_3O_4@SiO_2-$(CH_2)_3$-Cl MNPs

To a solution of 1,3-phenylenediamine (1.3 g, 0.012 mol) and a few drops of triethylamine as a base in ethanol (70 ml), Fe_3O_4@SiO_2-$(CH_2)_3$-Cl (1 g) was added to obtain a suspension in 15 min. The resulting mixture was refluxed in N_2 for 24 hr and the final precipitate as the product was separated with a magnet, washed three times with ethanol and dried at room temperature.

2.2.4 | Conversion of Fe_3O_4@SiO_2-$(CH_2)_3$-NH-(3-$NH_2C_6H_4$ into iminomethyl/phenol Schiff-base derivative (Fe_3O_4@SiO_2-iminomethyl/phenol)

Above-prepared Fe_3O_4@SiO_2-$(CH_2)_3$-NH-(3-$NH_2C_6H_4$) nanoparticles (1 g) were dispersed in 50 ml of methanol

in 15 min and was heated to reflux point. Then, to this suspension was added dropwise a solution of salicylaldehyde (2.93 g, 24 mmol) in ethanol (30 ml) using a decanter funnel. The reaction mixture was refluxed for 24 hr and the precipitated Fe_3O_4@SiO_2-Iminomethyl/phenol nanoparticles were separated using a magnet, washed repeatedly with ethanol, and dried in an oven.

2.2.5 | Preparation of the Fe_3O_4-immobilized Schiff-base Cu(II) complex Fe_3O_4@SiO_2-imine/phenoxy-Cu(II)

To a dispersion of previously prepared Fe_3O_4@SiO_2-iminomethyl/phenol nanoparticles (1 g) in ethanol (50 ml) was added dropwise a 5% (*w*/*v*) solution of Cu $(OAc)_2$ in ethanol (5 ml) and the resulting mixture was refluxed for 48 hr. After the reaction completed, the expected Fe_3O_4@SiO_2-iminomethyl/phenol nanoparticles were magnetically separated by using a magnet. Finally, the isolated nanoparticles were washed repeatedly with ethanol and water to remove the remaining unreacted materials, and dried at 80 °C for 6 hr.

2.3 | General procedure for synthesis of 2-amino-4*H*-chromene derivatives 7–10

To a mixture of aromatic aldehyde **1** (1.0 mmol), malononitrile **2** (0.067 g, 1 mmol) and phenolic reagent (α-naphthol **3**, β-naphthol **4**, resorcinol **5** or 2-hydroxy-naphthalene-1,4-dione **6)** (1.0 mmol), catalyst, Fe_3O_4@SiO_2-imine/phenoxy-Cu(II) (0.02 g), was added. The mixture was stirred with a magnetic stirrer and heated at 80 °C under solvent-free conditions for an appropriate time until the mixture turned into solid (Table 1). After completion of the reaction, judged by TLC, the resulting reaction mixture was cooled to room temperature, diluted with hot ethanol (20 ml), and the catalyst was separated by an external magnet. The precipitated product was isolated by filtration and purified by recrystallization in hot ethanol.

2.4 | Selected data

2.4.1 | 3-Amino-4-phenyl-4*H*-benzo[*h*]chromene-2-carbonitrile (7 a)

Light brown; m.p. 220–222 °C; yield 91%; FT-IR (KBr) ν: 3474, 3305, 3189, 3055, 3021, 2202, 1711, 1656, 1632, 1574, 1375, 1262, 1186, 1012, 742 cm^{-1}; ^{1}H-NMR (90 MHz, DMSO-d_6) δ: 8.30–8.12 (m, 3H, H-Ar), 7.93–7.57 (m, 7H, H-Ar), 7.31–7.09 (m, 3H, H-Ar and NH_2), 5.20 (s, 1H, C-H) ppm.

TABLE 1 X-ray diffraction (XRD) data for and Fe_3O_4-SiO_2-Schiff base complex of Cu(II)-MNPs

Entry	2θ	Peak width [FWHM] (degree)	Size (nm)	interplanar spacing of the crystal (nm)
1	6.8	0.5	15.89	1.30
2	9.2	0.2	40.75	0.96
3	11.9	0.3	27.76	0.77
4	12.7	0.3	26.72	0.70
5	22	0.5	16.10	0.40
6	35.7	0.9	9.24	0.25

2.4.2 | 3-Amino-4-(2,6-dichlorophenyl)-4*H*-benzo[*h*]chromene-2-carbonitrile (7 b)

Brown; m.p. 212–214 °C; yield 96%; FT-IR (KBr) ν: 3591, 3476, 3328, 3196, 2192, 1662, 1637, 1557, 1437, 1292, 1103, 845, 747 cm^{-1}; ^{1}H-NMR (90 MHz, DMSO-d_6) δ: 8.26–7.24 (m, 9H, Ar-H), 6.82 (s, 2H, NH_2), 5.95 (s, 1H, C-H) ppm.

2.4.3 | 3-Amino-4-(4-chloro-3-nitrophenyl)-4*H*-benzo[*h*]chromene-2-carbonitrile (7 c)

Light brown; m.p. 212–214 °C; yield 97%; FT-IR (KBr) ν: 3473, 3328, 3196, 3068, 2194, 1669, 1603, 1570, 1535, 1411, 1377, 1260, 1190, 806, 754 cm^{-1}; ^{1}H-NMR (400 MHz, DMSO-d_6) δ: 8.25 (d, J = 8.24 Hz, 1H, Ar-H), 8.03 (d,, J = 1.7 Hz, 1H, Ar-H), 7.90 (d, J = 8.01 Hz, 1H, Ar-H), 7.72 (d, J = 8.01 Hz, 1H, Ar-H), 7.66–7.57 (m, 4H, Ar-H), 7.34 (s, 2H, NH_2), 7.13 (d, J = 8.52 Hz, 1H, Ar-H), 5.15 (s,1H, C-H) ppm; ^{13}C-NMR (100 MHz, DMSO-d_6) δ: 160.3, 147.6, 146.6, 142.9, 133.2, 132.9, 132.1, 127.7, 127.0, 126.8, 125.8, 124.5, 124.2, 123.5, 122.7, 120.8, 120.1, 116.2 ppm. ESI-MSM/Z = 376.9 $[M]^+$.

2.4.4 | 3-Amino-4-(4-methoxyphenyl)-4*H*-benzo[*h*]chromene-2-carbonitrile (7 d)

Cream; m.p. 198–200 °C; yield 90%; FT-IR (KBr) ν: 3417, 3326, 3203, 2907, 2837, 2194, 1606, 1509, 1408, 1290, 1191, 1024, 809, 743 cm^{-1}; ^{1}H-NMR (90 MHz, DMSO-d_6) δ: 8.28–6.91 (m, 10H, Ar-H), 6.82 s, 2H, NH_2), 4.8 (s, 1H, C-H), 3.71 (s, 3H, OCH_3) ppm.

2.4.5 | 3-Amino-4-(4-hydroxyphenyl)-4*H*-benzo[*h*]chromene-2-carbonitrile (7 e)

Brown; m.p. 241–243 °C; yield 97%; FT-IR (KBr) ν: 3457, 3316, 3192, 2198, 1630, 1511, 1448, 1261, 1039, 854, 749 cm^{-1}; ^{1}H-NMR (90 MHz, DMSO-d_6) δ: 9.32 (s, 1H, OH), 8.26–6.37 (m, 10H, Ar-H), 6.64 (s, 2H, NH_2), 4.77 (s, 1H, C-H) ppm.

2.4.6 | 3-Amino-4-phenyl-1*H*-benzo[*f*]chromene-2-carbonitrile (8 a)

Light brown; m.p. 270–272 °C; yield 93%; FT-IR (KBr) ν: 3434, 3339, 3193, 3022, 2885, 2183, 1639, 1517, 1284, 815, 610 cm^{-1}; ^{1}H-NMR (90 MHz, DMSO-d_6) δ: 8.29–8.17 (d, 1H, Ar-H), 7.89–7.83 (d, 1H, Ar-H), 7.61–7.53 (m, 3H, Ar-H), 7.04–7.25 (m, 9H, Ar-H and NH_2), 4.88 (s, 1H, C-H) ppm.

2.4.7 | 3-Amino-4-(2,4-dichlorophenyl)-1*H*-benzo[*f*]chromene-2-carbonitrile (8 b)

Light Brown; m.p. 228–230 °C; yield 96%; FT-IR (KBr) ν: 3463, 3324, 3190, 2200, 1662, 1557, 1408, 1260, 1187, 1046, 846, 741 cm^{-1}; ^{1}H-NMR (400 MHz, DMSO-d_6) δ: 7.94 (dd, J = 22.6, 8 Hz, 2H, Ar-H), 7.62 (d, J = 1.7 Hz, 1H, Ar-H), 7.56 (d, J = 8.3 Hz, 1H, Ar-H) 7.49–7.40 (m, 2H, Ar-H), 7.33 (d, 1H, J = 8.9 Hz, Ar-H), 7.26 (dd, J = 10,1.7 Hz, 1H, Ar-H), 7.11 (s, 2H, NH_2), 7.00 (d, J = 8.2 Hz, 1H, Ar-H), 5.69 (s, 1H, C-H) ppm; ^{13}C-NMR (100 MHz, DMSO-d_6) δ: 159.8, 147.1, 141.6, 132.0, 131.9, 131.4, 130.7, 130.0, 129.9, 128.9, 128.7, 128.4, 127.5, 125.1, 122.5, 119.6, 116.8, 114.1 ppm.

2.4.8 | 2-Amino-7-hydroxy-4-phenyl-4*H*-chromene-3-carbonitrile (9 a)

Brown; m.p. 238–240 °C; yield 92%; FT-IR (KBr) ν: 3495, 3424, 3220, 2193, 1654, 1506, 1454, 1302, 1114, 806, 623 cm^{-1}; ^{1}H-NMR (90 MHz, DMSO-d_6) δ: 9.69 (s, 1H, OH), 7.24–7.19 (m, 5H, Ar-H), 6.86–6.75 (m, 3H, Ar-H), 6.51–6.41 (s, 2H, NH_2), 4.61 (s, 1H, C-H) ppm.

2.4.9 | 2-Amino-7-hydroxy-4-(3-nitrophenyl)-4*H*-chromene-3-carbonitrile (9 b)

Dark brown; m.p. 165–167 °C; yield 94%; FT-IR (KBr) ν: 3472, 3342, 3104, 2195, 1643, 1588, 1460, 1156, 855, 792 cm^{-1}; ^{1}H-NMR (90 MHz, DMSO-d_6) δ: 9.78 (s, 1H, OH), 8.04–6.82 (m, 7H, Ar-H), 6.47 (s, 2H, NH_2), 4.93 (s, 1H, C-H) ppm.

2.4.10 | 2-Amino-4-(2,4-dichlorophenyl)-7-hydroxy-4*H*-chromene-3-carbonitrile (9 c)

White solid; m.p. 263–265 °C; yield 97%; FT-IR (KBr) ν: 3480, 3341, 3276, 3216, 2194, 1642, 1587, 1412, 1153, 844 cm^{-1}; ^{1}H-NMR (400 MHz, DMSO-d_6) δ: 9.80 (s, 1H, OH), 7.57 (d, J = 2 Hz, 1H, Ar-H), 7.39 (dd, J = 8.4, 2 Hz, 1H, Ar-H), 7.21 (d, J = 8.4 Hz, 1H, Ar-H), 6.98 (s, 2H, NH_2), 6.71 (d, J = 8.5 Hz, 1H, Ar-H), 6.48 (dd, J = 8.4, 2.4 Hz, 1H, Ar-H), 6.41 (d, J = 2.2 Hz, 1H, Ar-H), 5.12 (s, 1H, C-H) ppm; ^{13}C NMR (100 MHz, DMSO-d_6) δ: 160.5, 157.4, 149.0, 141.8, 132.8, 132.2, 129.2, 129.1, 128.0, 120.1, 120.1, 112.6, 111.9, 102.3 ppm.

2.4.11 | 2-Amino-7-hydroxy-4-(thiophen-2-yl)-4*H*-chromene-3-carbonitrile (9 d)

Cream solid; m.p. 240–242 °C; yield 97%; FT-IR (KBr) ν: 3476, 3423, 3332, 3219, 2195, 1654, 1588, 1506, 1327, 1290, 1150, 1043, 867 cm^{-1}; ^{1}H-NMR (400 MHz, DMSO-d_6) δ: 9.78 (s, 1H, OH), 7.34 (d, J = 4.9 Hz, 1H, Ar-H), 6.96 (d, J = 4.6 Hz, 2H, Ar-H), 6.95 (s, 2H, NH_2), 6.91 (t, J = 4 Hz, 1H, Ar-H), 6.53 (dd, J = 8.3, 2.1 Hz, 1H, Ar-H), 6.39 (d, J = 2.1 Hz, 1H, Ar-H), 4.98 (s, 1H, C-H) ppm; ^{13}C NMR (100 MHz, DMSO-d_6) δ: 160.3, 157.3, 151.5, 148.5, 129.8, 126.8, 125.0, 124.0, 120.5, 120.5, 113.5, 112.4, 102.2 ppm.

2.4.12 | 2-Amino-4-(4-fluorophenyl)-7-hydroxy-4*H*-chromene-3-carbonitrile (9 e)

Brown solid; m.p. 202–204 °C; yield 96%; FT-IR (KBr) ν: 3432, 3344, 3281, 2187, 1646, 1505, 1407, 1094, 865, 779 cm^{-1}; ^{1}H-NMR (90 MHz, DMSO-d_6) δ: 9.71 (s, 1H, OH), 7.19–6.51 (m, 7H, Ar-H), 6.41 (s, 2H, NH_2), 4.65 (s, 1H, C-H) ppm.

2.4.13 | 2-Amino-7-hydroxy-4-(4-tolyl)-4*H*-chromene-3-carbonitrile (9 f)

Brown solid; m.p. 202–204 °C; yield 90%; FT-IR (KBr) ν: 3440, 3339, 3049, 2972, 2191, 1641, 1589, 14.64, 1113, 1045, 858 cm^{-1}; ^{1}H-NMR (90 MHz, DMSO-d_6) δ: 9.33 (s, 1H, OH), 8.46–6.50 (m, 7H, Ar-H), 6.41 (s, 2H, NH_2), 2.25 (s, 3H, CH_3) ppm.

2.4.14 | 2-Amino-5,10-dioxo-4-phenyl-5,10-dihydro-4*H*-benzo[g]chromene-3-carbonitrile (10 a)

Brown solid; m.p. 263–265 °C; yield 91%; FT-IR (KBr) ν: 3400, 3323, 3191, 3021, 2198, 1670, 1405, 1244, 984, 754 cm^{-1}; ^{1}H-NMR (90 MHz, DMSO-d_6) δ: 8.02–7.84 (m, 4H, Ar-H), 7.30–6.87 (m, 7H, Ar-H and NH_2), 4.61 (s, 1H, C-H) ppm.

2.4.15 | 2-Amino-5,10-dioxo-4-(4-nitrophenyl)-5,10-dihydro-4*H*-benzo[g]chromene-3-carbonitrile (10 b)

Dark-brown solid; m.p. 232–234 °C; yield 97%; FT-IR (KBr) ν: 3397, 3331, 3196, 3075, 2203, 1670, 1521, 1411, 1246, 1183, 859, 780 cm^{-1}; ^{1}H-NMR (90 MHz, DMSO-d_6) δ: 8.21–7.60 (m, 8H, Ar-H), 7.47 (s, 2H, NH_2), 4.82 (s, 1H, C-H) ppm.

2.4.16 | 2-Amino-4-(2,4-dichlorophenyl)-5,10-dioxo-5,10-dihydro-4*H*-benzo[g]chromene-3-carbonitrile (10 c)

Red-brown solid; m.p. 280–282 °C; yield 97%; FT-IR (KBr) ν: 3467, 3341, 3167, 3073, 2202, 1670, 1592, 1248, 1199, 847, 717 cm^{-1}; ^{1}H-NMR (90 MHz, DMSO-d_6) δ: 8.35–7.25 (m, 9H, Ar-H and NH_2), 5.12 (s, 1H, C-H) ppm.

2.4.17 | 2-amino-4-(4-chloro-3-nitrophenyl)-5,10-dihydro-5,10-dioxo-4*H*-benzo[g]chromene-3-carbonitrile (10 d)

Red-brown solid; m.p. 255–257 °C; yield 98%; FT-IR (KBr) ν: 3410, 3330, 3218, 2193, 1660, 1593, 1530, 1412, 1245, 716 cm^{-1}; ^{1}H-NMR (400 MHz, DMSO-d_6) δ: 8.08 (s, 1H, Ar-H), 8.06 (dd, J = 6.5, 2 Hz, 1H, Ar-H) 7.88–7.71 (m, 5H, Ar-H), 7.50 (s, 2H, NH_2), 4.81 (s, 1H, C-H) ppm; ^{13}C-NMR (100 MHz, DMSO-d_6) δ: 182.6, 176.9, 158.2, 149.5, 148.1, 134.5, 134.1, 131.1, 131.0, 130.5, 128.3, 126.0, 125.7, 122.6, 122.6, 119.5, 119.5, 112.4 ppm. ESI-MS-M/Z = 406.9 $[M]^+$.

2.4.18 | 2-Amino-4-(furan-2-yl)-5,10-dioxo-5,10-dihydro-4*H*-benzo[g]chromene-3-carbonitrile (10 e)

Orange solid; m.p. 257–259 °C; yield 97%; FT-IR (KBr) ν: 3414, 3330, 2197, 1665, 1592, 1420, 1201, 708 cm^{-1}; ^{1}H-NMR (400 MHz, DMSO-d_6) δ: 8.04 (dd, J = 5.7, 3.3 Hz, 1H, Ar-H), 7.95–7.84(m, 3H, Ar-H), 7.53(d, J = 1 Hz, 1H, Ar-H), 7.43 (s, 2H, NH_2), 6.36 (dd, J = 3.1, 1.9 Hz, 1H, Ar-H), 6.29 (d, J = 3.18 Hz, 1H, Ar-H), 4.76 (s, 1H, C-H) ppm; ^{13}C-NMR (100 MHz, DMSO-d_6) δ: 182.2, 176.8, 159.2, 154.5, 149.2, 142.7, 134.7, 130.9, 130.5, 126.2, 125.9, 119.8, 119.7, 119.2, 119.2, 110.7, 106.4 ppm.

2.4.19 | 2-Amino-4-(4-dimethylaminophenyl)-5,10-dioxo-5,10-dihydro-4*H*-benzo[g]chromene-3-carbonitrile (10 f)

Dark-orange solid; m.p. 241–243 °C; yield 94%; FT-IR (KBr) ν: 3336, 3323, 3193, 2798, 2199, 1667, 1524, 1403, 1244, 715 cm^{-1}; ^{1}H-NMR (400 MHz, DMSO-d_6) δ: 8.04–8.02 (m, 1H, Ar-H),7.88–7.81 (m, 3H, Ar-H), 7.25 (s, 2H, NH_2), 7.08 (d, J = 8 Hz, 2H, Ar-H), 6.63 (d, J = 8.7 Hz, 2H, Ar-H), 4.48 (s, 1H, C-H), 2.83 (s, 6H, CH_3) ppm; ^{13}C-NMR (100 MHz, DMSO-d_6) δ: 182.6, 176.9, 158.2, 149.5, 148.1, 134.5, 134.1, 131.1, 131.0, 130.5, 128.3, 126.0, 125.0, 122.6, 122.6, 119.5, 119.5, 112.4 ppm. ESI-MS-M/Z = 371 $[M]^+$.

2.4.20 | 2-Amino-5,10-dioxo-4-(4-tolyl)-5,10-dihydro-4*H*-benzo[g]chromene-3-carbonitrile (10 g)

Dark-brown; m.p. 243–245 °C; yield 94%; FT-IR (KBr) ν: 3407, 3327, 3195, 3247, 2199, 1661, 1593, 1408, 1243, 950, 734 cm^{-1}; ^{1}H-NMR (90 MHz, DMSO-d_6) δ: 7.99–7.14 (m, 10H, Ar-H and NH_2), 4.44 (s, 1H, C-H), 2.25 (s, 6H, CH_3) ppm.

3 | RESULTS AND DISCUSSION

3.1 | Preparation of the Fe_3O_4@SiO_2-imine/phenoxy-Cu(II) catalyst

Herin, we report the stepwise synthesis of hitherto unexplored Fe_3O_4-supported copper (II) Schiff-base complex Fe_3O_4@SiO_2-imine/phenoxy-Cu(II) as an efficient and recyclable nanocatalyst as explained above (Scheme 2).

First, the silica-coated Fe_3O_4 MNPs were prepared by co-precipitation of ferrous (Fe^{2+}) and ferric (Fe^{3+}) ions followed by the reaction of dispersion of the resulted nanoparticles in ethanol and deionized water with tetraethyl orthosilicate (TEOS) in the presence of 25% ammonia solution to obtain the core-shell Fe_3O_4@SiO_2

nanoparticles. In the next step, the Fe_3O_4@SiO_2 nanoparticles were reacted with (3-chloropropyl) triethoxysilane (CPTES) in dry toluene under nitrogen atmosphere to obtain the chloro-functionalized Fe_3O_4@SiO_2-$(CH_2)_3$-Cl MNPs. Then, the reaction of Fe_3O_4@SiO_2-$(CH_2)_3$-Cl nanoparticles with 1,3-phenylenediamine in ethanol containing few drops of triethylamine under nitrogen atmosphere and refluxed condition furnished the Fe_3O_4@SiO_2-$(CH_2)_3$-NH-(3-$NH_2C_6H_4$) nanoparticles. Conversion of the Fe_3O_4@SiO_2-$(CH_2)_3$-NH-(3-$NH_2C_6H_4$ nanoparticles into iminomethyl/phenol Schiff-base derivative Fe_3O_4@SiO_2-Iminomethyl/phenol was accomplished via the reaction of Fe_3O_4@SiO_2-$(CH_2)_3$-NH-(3-$NH_2C_6H_4$) nanoparticles as a dispersion in methanol with salicylaldehyde in ethanol under refluxed condition and nitrogen atmosphere to obtain the Fe_3O_4@SiO_2-Iminomethyl/phenol MNPs. Finally, the dispersion of Fe_3O_4@SiO_2-Iminomethyl/phenol nanoparticles in ethanol was treated with 5% (*w*/*v*) solution of $Cu(OAc)_2$ in ethanol to afford the Fe_3O_4-immobilized Schiff-base Cu(II) complex Fe_3O_4@SiO_2-imine/phenoxy-Cu (II). The structure of Fe_3O_4@SiO_2-imine/phenoxy-Cu(II) MNPs was fully established by different analytical techniques as described below.

3.2 | Characterization of the Fe_3O_4@SiO_2-imine/phenoxy-Cu(II) catalyst

The structure of Fe_3O_4@SiO_2-imine/phenoxy-Cu (II) catalyst was fully established by different analytical techniques as described below. The characterization data for the catalyst are available at the end of the article.

3.2.1 | FT-IR analysis

The FT-IR spectra of the naked Fe_3O_4 NPs (a), silica-coated Fe_3O_4@SiO_2 NPs (b), Fe_3O_4@SiO_2-$(CH_2)_3$-Cl (c), Fe_3O_4@SiO_2-$(CH_2)_3$-NH-(3-$NH_2C_6H_4$ (d), Fe_3O_4@SiO_2-iminomethyl/phenol (e) and Fe_3O_4@SiO_2-imine/phenoxy-Cu(II) (f) presented in Figure 1 are compared. Appearance of the characteristic absorption bands at about 566 and 637 cm^{-1} corresponding to the Fe-O vibrations in all the spectra **1a-f** indicated the successful immobilization of the organic moieties and Cu species on the surface of the Fe_3O_4 nanoparticles. In addition, a broad peak at 3000–3600 cm^{-1} exhibited by these spectra along with another peak at about 1612 cm^{-1} are associated with the O-H stretching vibrations.[67,68] The absorption band observed at about 1084 cm^{-1} with a small shoulder at 1180 cm^{-1} in the spectra **1b-f** can be attributed to the symmetric and asymmetric stretching vibrations of the Si-O-Si groups which clearly confirm the silica-modification of the nanoparticles. Moreover, the presence of σ-bonded propyl groups on the surface of the Fe_3O_4 was confirmed by the aliphatic C-H stretching vibrations at 2949–2878 cm^{-1} observed in the spectra **1c-f.** Immobilization of the 1,3-phenylendiamine on the surface of the silica-coated Fe_3O_4 nanoparticles was evidenced by the presence of the characteristic N-H stretching band at 3292 cm^{-1} overlapped with the O-H group in the spectrum **1 d**. Formation of the immobilized iminomethyl/phenol Schiff-base ligand and its Cu (II) complex were approved by the N-H and C=N characteristic vibrational bands at about 3292 and 1629 cm^{-1} respectively as observed in the spectra **1 e** and **1 f**. Moreover, the absorption band observed at 459 cm^{-1} in the

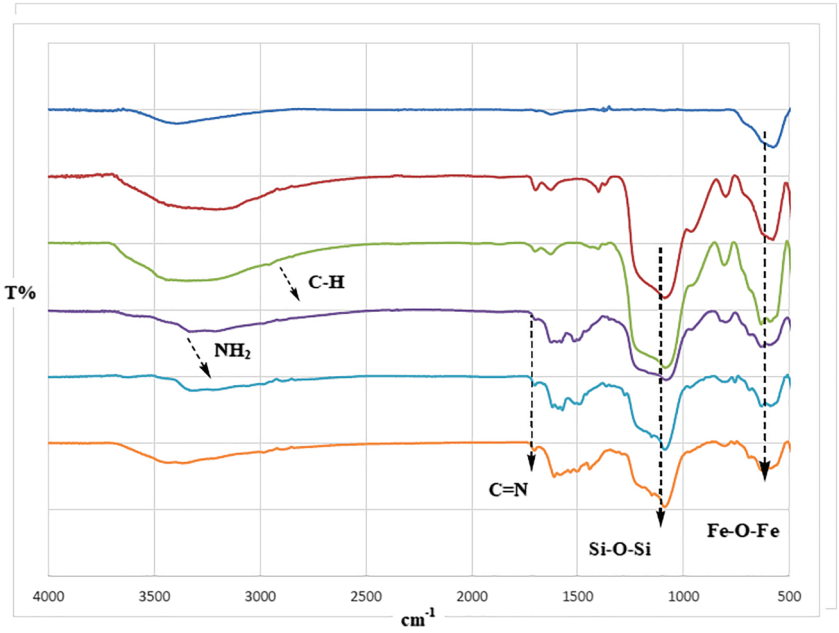

FIGURE 1 FT-IR spectra of (a) naked Fe_3O_4, (b) Fe_3O_4@SiO_2, (c) Fe_3O_4@SiO_2-$(CH_2)_3$-Cl, (d) Fe_3O_4@SiO_2-$(CH_2)_3$-NH-(3-$NH_2C_6H_4$, (e) Fe_3O_4@SiO_2-iminomethyl/phenol and (f) Fe_3O_4@SiO_2-Imine/Phenoxy-Cu(II)

spectrum **1 f** can be attributed to the Cu-O stretching vibration. Appearance of additional bands in the range 1170–1600 cm^{-1} can be assigned to the stretching vibrations of the C=C, C-N, and C-O bonds which further confirm the formation immobilized Schiff-base ligand and its related Cu (II) complex. The slight shift of the C=N absorption frequency to a lower frequency shown in the spectrum **1 f** is likely due to the successful co-ordination of the imminomethyl/phenol Schiff-base ligand to Cu(II) ion.[69]

3.2.2 | XRD analysis

The crystalline nature and the size of the Fe_3O_4@SiO_2-imine/phenoxy-Cu(II) nanoparticles were determined by X-ray diffraction (XRD) analysis. As indicated in the resulted XRD pattern of the Fe_3O_4@SiO_2-imine/phenoxy-Cu(II) nanoparticles in Figure 2a, the intense Bragg's peaks observed at 2θ = 18.5°, 30.5°, 35.7°, 43.3°, 53.8°, 57.1°, 62.8 and 73.8° (2 a) correspond to the (111), (220), (311), (400), (422), (511) and (531) reflection planes, respectively. These peaks are related to the crystal planes in the Fe_3O_4 lattice. The positions and relative intensities of these peaks clearly match with the literature data from the Joint Committee on Powder Diffraction System of Fe_3O_4 (JCPDS Card No. 65–3107). Comparison of the XRD pattern of Fe_3O_4@SiO_2-imine/phenoxy-Cu(II) nanoparticles (2 a) with that of the blank Fe_3O_4 nanoparticles (2 b) proved that the crystalline structure was retained in the Fe_3O_4@SiO_2-imine/phenoxy-Cu(II) nanoparticles after coatation with SiO_2 layer and immobilization with the Schiff-base Cu (II) complex.[70]

From the XRD pattern can be ascertained the average crystallite size of nanoparticles by applying the Debye–Scherer equation that can be written as: ((D = (Kλ)/(βcosθ)).[71] In this equation, D is the average crystalline and K is a dimensionless shape factor. The shape factor has a typical value of about 0.9, which varies with the actual shape of the crystallite; λ is the X-ray wavelength, β is the line broadening at half the maximum intensity (FWHM) after subtracting the instrumental line broadening in radians, and also θ is the Bragg angle. Eventually, Bragg equation ($d_{hkl} = \lambda/2\sin\theta$) was employed to calculate the distance between the layers (Table 1).

3.2.3 | Energy dispersive X-ray (EDX) and inductively coupled plasma (ICP) analyses

The elemental composition of Fe_3O_4@SiO_2-imine/phenoxy-Cu(II) nanoparticles was determined by EDX.

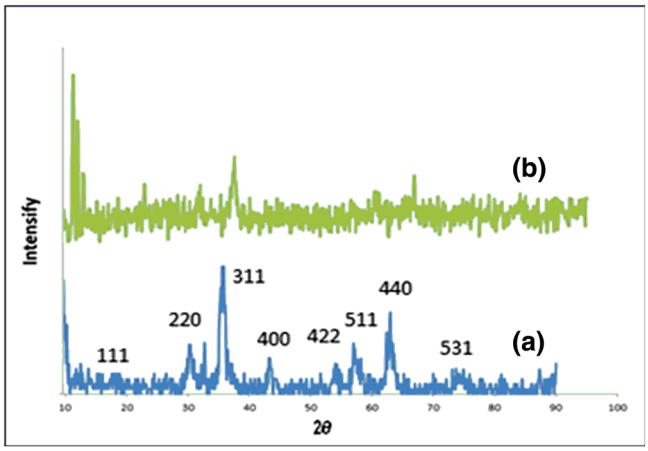

FIGURE 2 XRD patterns of (a) naked Fe_3O_4 MNPs and (b) Fe_3O_4@SiO_2-imine/Phenoxy-Cu(II) MNPs

The presence of Fe, Si, O, N, C and Cu elements with the corresponding weight percent (0.81%, 77%, 0.32%, 0.20%, 0.18%, 0.7%) is clearly evidenced by the EDX spectrum presented in Figure 3. Formation of the Iminomethyl/Phenol Schiff-base and its Cu(II) complex grafted on the surface of the nanoparticles was confirmed by appearance of the peaks due to the N and Cu atoms. In addition, the Cu content of the catalyst was detected and evaluated by ICP-OES which was found to be 11.36 wt%.

3.2.4 | Scanning electron microscopy (SEM) and transmission electron microscopy (TEM)

The morphology and particle size of the Fe_3O_4@SiO_2-imine/phenoxy-Cu(II) nanoparticles were studied by field-emission scanning electron microscopy (FE-SEM) and TEM, respectively. It can be observed from the TEM images shown in Figure 4a that, the encapsulated Fe_3O_4@SiO_2-imine/phenoxy-Cu(II) complex are made up of nanometer-sized particles exhibiting a regularly spherical morphology with the diameters in the range 15–20 nm. Moreover, on the basis of the TEM image shown in Figure 4b, the core-shell structure and the nanometer-sized nature of the Fe_3O_4@SiO_2-imine/phenoxy-Cu(II) particles were obvious. Also, the core-shell structure of the nanoparticles was further approved by the presence of dark spots inside the bright spherical thin silica shell. However, it should be noted that, due to aggregation of the particles with paramagnetic nature, the exact evaluation of the particle size is difficult.

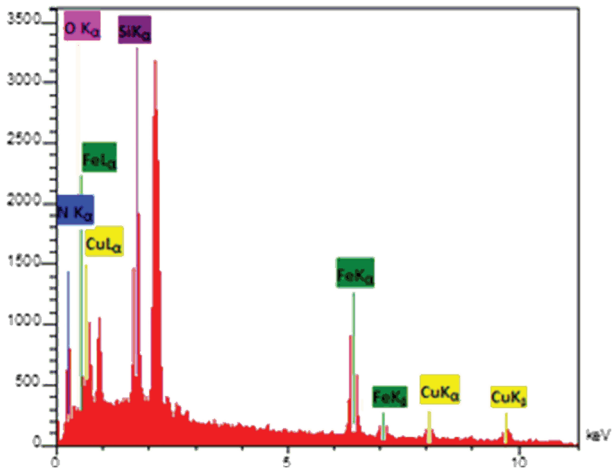

FIGURE 3 The energy dispersive X-ray (EDX) spectrum of Fe_3O_4@SiO_2-imine/Phenoxy-Cu(II) MNPs

3.2.5 | Study of X-ray photoelectron spectroscopy (XPS) of the synthesized Fe_3O_4@SiO_2-imine/phenoxy-Cu(II) nanoparticles

X-ray photoelectron spectroscopy (XPS), also known as electron spectroscopy for chemical analysis (ESCA), is used to determine quantitative atomic composition and chemistry of the Fe_3O_4@SiO_2-imine/phenoxy-Cu(II) nanoparticles. The discrete peaks observed in the XPS spectra determined in the regions for Si, Fe, N, Fe (Figure 5) correspond to ionization from the core electron orbitals of the atoms in the outermost 10–50 Å of the surface. The results obtained from the analysis of the Si 2p spectra confirmed the presence of binding energies at 103.28 and 103.88 eV corresponding to Si-O-Si and Si-O bonds respectively. Also, the presence of carbon atom in the structure of the nanoparticles was approved by the peaks related to C 1 s at the binding energies of 284.88 (C-O-C), 286.18 (C-O) and 287.58 (C=N) eV.[72] The nitrogen atoms contained in the grafted Schiff-base group exhibited their N 1 s peaks at the related binding energies 398.68 and 400.28 eV corresponding to C-N and C=N bonds respectively.[73] Appearance of the Fe 2p3/*2* and Fe 2p1/*2* peaks binding energies at 712.68 and *725.38 eV* respectively correspond to Fe^{3+} present in the Fe_3O_4 phase. The XPS spectrum resulted in the Fe 2 pv region presented two main binding energy peaks at 710.68 and 724.6 eV which were related to Fe^{2+}.[74]

XPS spectrum in the Cu2p region showed a doublet peak located at approximately 933.48 and 952.18 eV which are attributed to Cu 2p3/2 and Cu 2p1/2

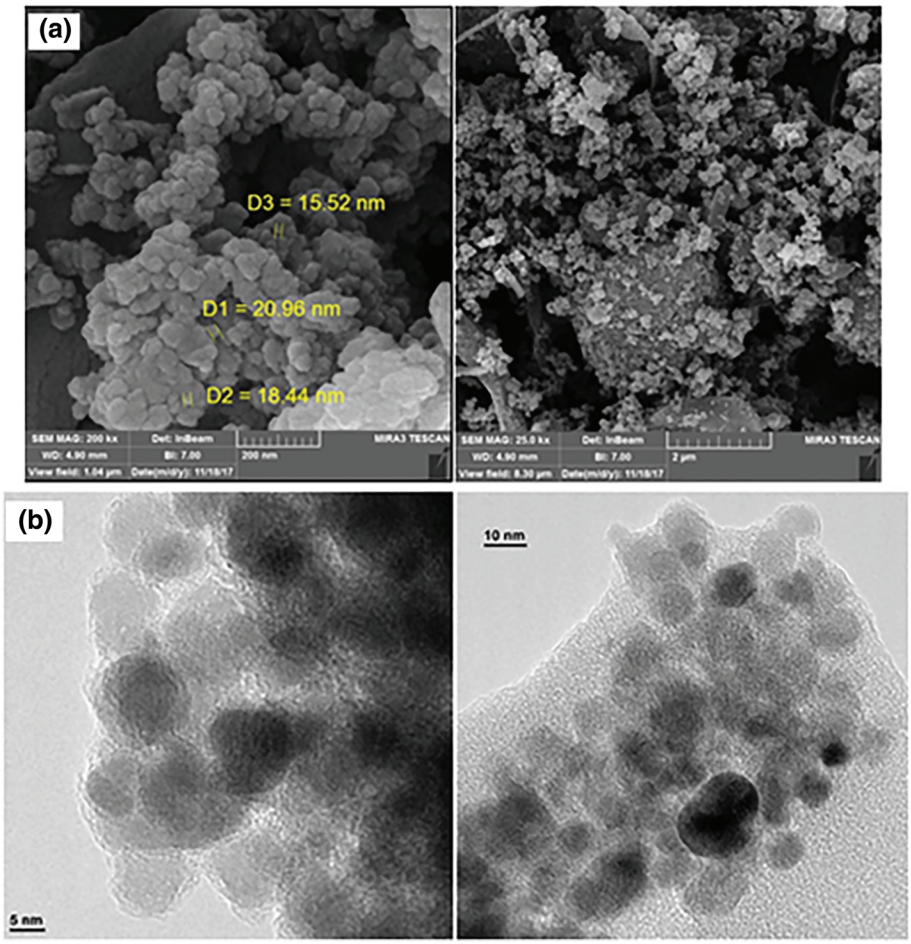

FIGURE 4 (a) SEM and (b) TEM images of the Fe_3O_4@SiO_2-imine/Phenoxy-Cu(II) MNPs

respectively Also, the doublet peaks with binding energies of 935.08 and 954.58 eV were assigned to Cu 2p3/2 and Cu 2p1/2 in Cu (II_ On the other hand, two shake-up satellite peaks at 941.28 and 944.48 eV are related to Cu (II) species.[75]

3.2.6 | Vibrating-sample magnetometer (VSM) analysis of Fe_3O_4@SiO_2-imine/phenoxy-Cu(II) nanoparticles

In addition to the above-mentioned XRD, SEM and TEM analyses, the room temperature magnetization behavior was also studied by conducting vibrating-sample magnetometer (VSM) on Fe_3O_4@SiO_2-imine/phenoxy-Cu(II) nanoparticles. The magnetization curves obtained for the naked Fe_3O_4 and Fe_3O_4@SiO_2-imine/phenoxy-Cu(II) nanoparticles are illustrated in Figure 6. As seen in these curves, the specific saturation magnetizations (Ms) of uncoated Fe_3O_4 and Fe_3O_4@SiO_2-imine/phenoxy-Cu(II) nanoparticles are measured to be 54 and 26 emu g^{-1} respectively. The slight decrease (28 emu g^{-1}) observed in the saturation magnetization value (Ms) of the Fe_3O_4@SiO_2-imine/phenoxy-Cu(II) nanoparticles compared to the Ms value of the bare Fe_3O_4 nanoparticles was most likely attributed to the existence of the coated SiO_2 and Schiff-base Cu(II) (11.36 wt.%) materials on the surface of the Fe_3O_4 nanoparticles.

3.2.7 | Thermal gravimetric analysis (TGA)

Thermal gravimetric analysis (TGA) was applied to the Fe_3O_4@SiO_2-imine/phenoxy-Cu(II) catalyst in order to investigate its thermal stability and verify the existence of the materials immobilized on the surface of the nanoparticles. According to the TGA pattern presented in Figure 7, weight loss takes place in three consecutive

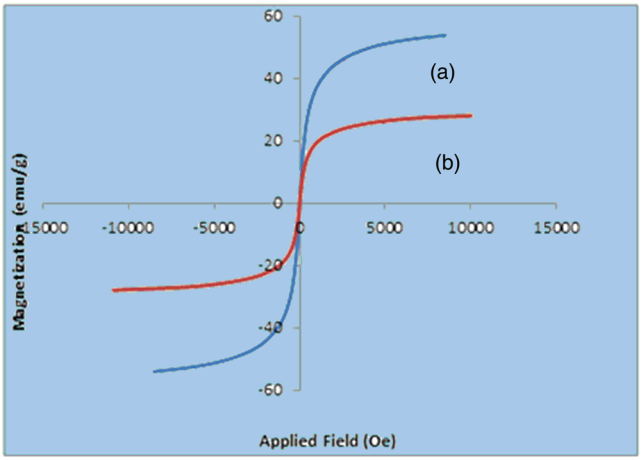

FIGURE 6 Magnetization curves of (a) bare Fe_3O_4 and (b) Fe_3O_4@SiO_2-imine/phenoxy-Cu(II)

steps in thermal range 25–800 °C. The first small weight loss of about 7% occurs below 150 °C which is likely due to the removal of the adsorbed water and remaining organic solvents. The second weight loss of almost 12% in the range 150–450 °C is possibly attributed to the removal of the Fe_3O_4-grafted organic materials and Cu (II) Schiff base complex. Complete decomposition of the catalyst and the possible change of the crystal phase from Fe_3O_4 to γ-Fe_2O_3 happen in the final thermal step beyond 450 °C.[76] These results clearly confirm the successful immobilization of the imine/phenoxy derived Schiff-base Cu (II) complex on the surface of the silica-coated Fe_3O_4 MNPs.

3.3 | Catalyst activity of Fe_3O_4@SiO_2-imine/phenoxy-Cu(II) MNPs

In order to evaluate the catalytic activity of the synthesized Fe_3O_4@SiO_2-imine/phenoxy-Cu(II) nanoparticles, we chose to study three-component condensation

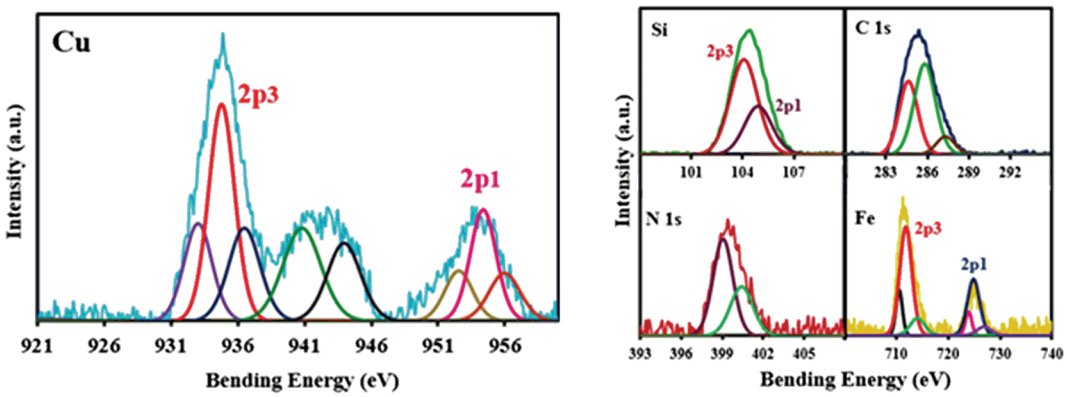

FIGURE 5 The X-ray photoelectron spectroscopy (XPS) spectra of the synthesized Fe_3O_4@SiO_2-Imine/Phenoxy-Cu(II) nanoparticles

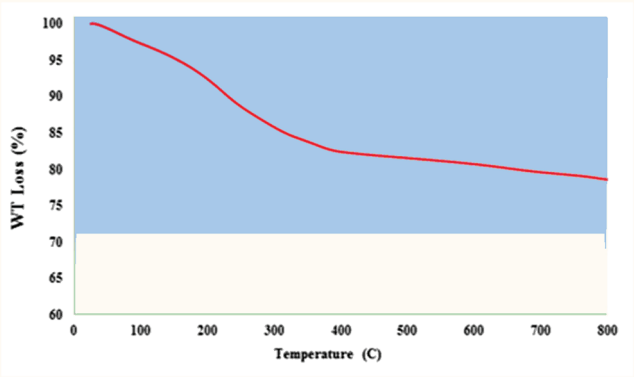

FIGURE 7 TGA curve of Fe_3O_4@SiO_2-imine/phenoxy-Cu (II) MNPs

reactions between the aldehydes, malononitrile, and different phenolic reagents like *α*-naphthol, *β*-naphthol, resorcinol, and 2-hydroxynaphthalene-1,4-dione to synthesis various derivatives of 2-amino-4*H*-chromene-3-carbonitrile using Fe_3O_4@SiO_2-imine/phenoxy-Cu(II) nanoparticles as the catalyst (Scheme 1). At first, the effects of different reaction parameters such as catalyst loading, solvent, and temperature on the reaction were screened to establish the conditions of the reactions using the reaction between benzaldehyde, malononitrile and α-naphthol as the model reaction. According to the experimental results summarized in Table 2, the best results in terms of the reaction yield and rate for the selected model reaction were observed when the reaction was performed at 70 °C under solvent-free condition using the catalyst loading of 20 mg (entry 10). Indispensable use of the catalyst Fe_3O_4@SiO_2-imine/phenoxy-Cu (II) in the reaction was established by conducting the reaction under the optimized conditions in the absence of the catalyst and noticed that no detectable amount of the product was produced after a long reaction time (entry 13). Moreover, the catalytic activity of the Fe_3O_4@SiO_2-

TABLE 3 Comparative catalytic activity of Fe_3O_4@SiO_2-Imine/phenoxy-Cu(II) nanoparticles under optimal conditions

Entry	Catalyst	Time (min)	Yield (%)
1	Fe_3O_4@SiO_2-Imine/ Phenoxy-Cu (II)	10	98
2	Fe_3O_4@SiO_2-Iminomethyl/ Phenol	30	80
3	Fe_3O_4@SiO_2	120	58
4	Fe_3O_4	35	70

TABLE 2 Screening the reaction parameters for the synthesis of 2-amino-4-phenyl-4*H*-benzo[*h*]chromene-3-carbonitrile (**7a**)[a]

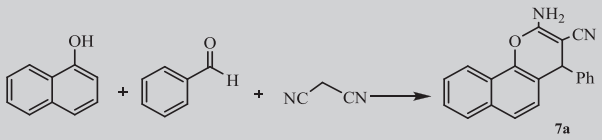

Entry	Catalyst (mg)	Solvent	Temperature (°C)	Time (min)	Yield (%)[b]
1	10	H_2O	25	80	38
2	10	EtOH	25	80	46
3	10	CH_3CN	25	80	43
4	10	Solvent-free	25	80	58
5	10	H_2O	reflux	60	45
6	10	EtOH	reflux	60	62
7	10	CH_3CN	reflux	60	68
8	10	Solvent-free	70	40	72
9	10	Solvent-free	100	40	70
10	**20**	**Solvent-free**	**70**	**10**	**98**
11	40	Solvent-free	70	15	85
12	60	Solvent-free	70	15	80
13	No catalyst	Solvent-free	70	120	trace

[a]Conditions: benzaldehyde (1 mmol), malononitrile (1 mmol), *α*-naphthol (1 mmol), solvent (5 ml).
[b]Isolated pure yield.

TABLE 4 Fe_3O_4@SiO_2-imine/phenoxy-Cu (II)-catalyzed synthesis of 2-amino-4*H*-chromene derivatives[a]

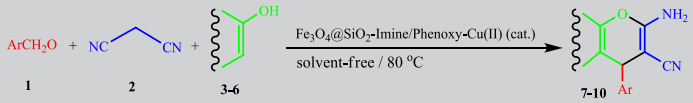

Entry	Ar	Phenols 3–6	Products 7–10	Time (min)	Yield (%)[b]	Mp (°C) Found	Mp (°C) Reported
1	C_6H_5	3	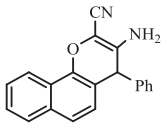 **7a**	10	98	210	205[77]
2	2,6-$Cl_2C_6H_3$	3	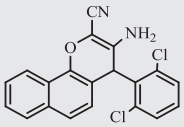 **7b**	8	96	212	214–216[27]
3[new]	4-Cl-3-$NO_2C_6H_3$	3	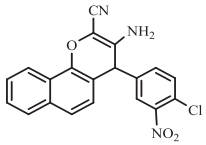 **7c**	8	97	258	-
4	4-$MeOC_6H_4$	3	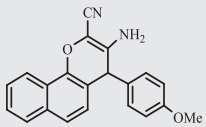 **7d**	12	90	200	195–196[29]
5	4-HOC_6H_4	3	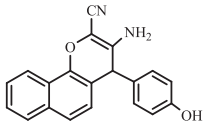 **7e**	12	92	241	245[77]

(Continues)

TABLE 4 (Continued)

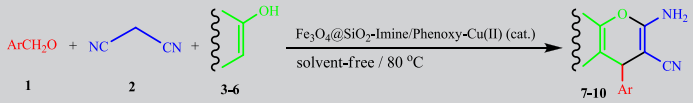

Entry	Ar	Phenols 3–6	Products 7–10	Time (min)	Yield (%)[b]	Mp (°C) Found	Mp (°C) Reported
6	C_6H_5	4	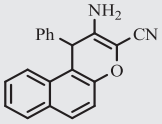 **8a**	10	93	270	274[77]
7	2,6-$Cl_2C_6H_3$	4	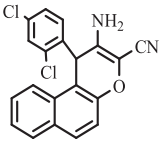 **8b**	8	96	230	222–224[29]
8	C_6H_5	5	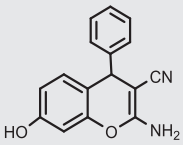 **9a**	12	92	238–240	234–237[30]
9	3-$NO_2C_6H_4$	5	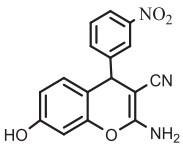 **9b**	13	94	165	169–170[31]
10	2,4-$Cl_2C_6H_3$	5	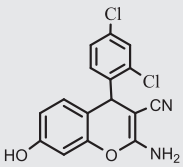 **9c**	10	97	263–265	256–258[71]

(Continues)

TABLE 4 (Continued)

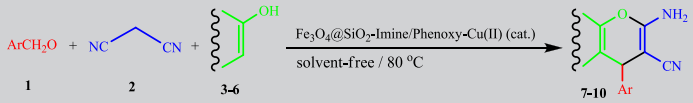

Entry	Ar	Phenols 3–6	Products 7–10	Time (min)	Yield (%)[b]	Mp (°C) Found	Mp (°C) Reported
11	Thiopen-2-yl	5	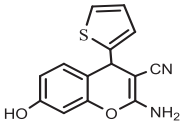 **9d**	10	96	240–242	230–232[71]
12	4-FC_6H_4	5	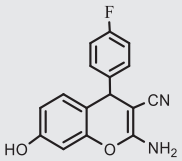 **9e**	9	96	202	186–188[78]
13	4-MeC_6H_4	5	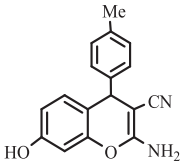 **9f** **9f**	14	90	178–180	183–186[30]
14	C_6H_5	6	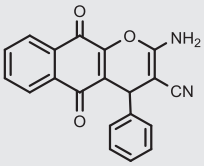 **10a**	10	91	265	260–26[79]
15	4-$NO_2C_6H_4$	6	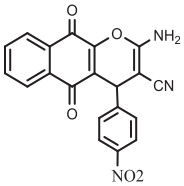 **10b**	9	97	232	233–234[79]

(Continues)

TABLE 4 (Continued)

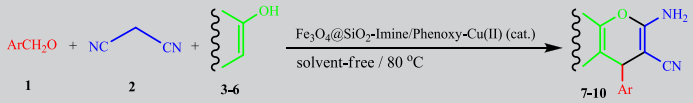

Entry	Ar	Phenols 3–6	Products 7–10	Time (min)	Yield (%)[b]	Mp (°C) Found	Mp (°C) Reported
16	4-ClC_6H_4	6	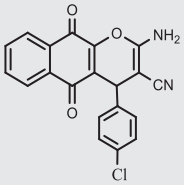 **10c**	8	97	250	252–254[80]
17[new]	4-Cl-3-$NO_2C_6H_3$	6	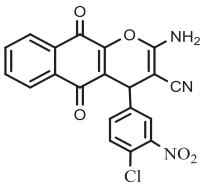 **10d**	8	98	255	-
18	Furan-2-yl	6	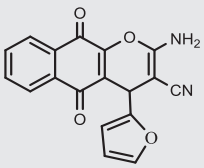 **10e**	8	97	262	266–268[76]
19[new]	4-$Me_2NC_6H_4$	6	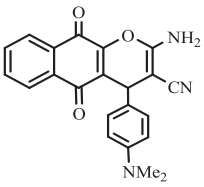 **10f**	10	94	243	-

(Continues)

TABLE 4 (Continued)

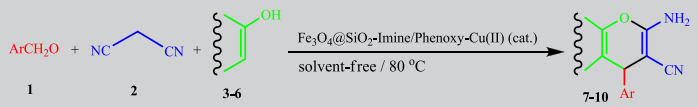

Entry	Ar	Phenols 3–6	Products 7–10	Time (min)	Yield (%)[b]	Mp (°C) Found	Mp (°C) Reported
20	4-MeC_6H_4	6	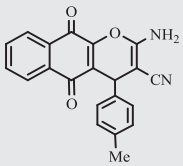 **10g**	12	89	245	242–244[80]

[a]Conditions: aldehyde (1 mmol), malononitrile (1 mmol), phenolic reagent (1 mmol), catalyst (0.02 g), 80 °C.
[b]Isolated pure yield.

imine/phenoxy-Cu(II) nanoparticles was compared with the catalytic activities of the bare Fe_3O_4, Fe_3O_4@SiO_2 and Fe_3O_4-supported Schiff-base nanoparticles in separate experiments conducted under the same optimal conditions. The resulting yields given in Table 3 clearly indicated that the Fe_3O_4@SiO_2-imine/phenoxy-Cu(II) nanoparticles perform relatively higher catalytic activity compared with other three nanoparticles.

With the optimized reaction conditions in hand, the scope and generality of the reaction was investigated using a divers series of aromatic aldehydes carrying different substituent groups and various phenolic compounds **4–6**. According to the experimental results summarized in Table 4, all the tested aldehydes reacted smoothly irrespective of the nature of the substituent groups and the resulted 2amino-4*H*-chromene derivatives **7a-e**, **8a-b**, **9a-f** and **10a-g** were produced in excellent yields and short reaction times. The products were structurally characterized by their physical properties and using FT-IR, ^{1}H NMR, ^{13}C NMR, and ESI-MS (in the case of new compounds) spectral analyses and compared with the reported data.

3.4 | Proposed catalytic reaction

A plausible mechanism for three-component reaction of aldehydes, malononitrile and different phenolic compounds for the synthesis of the corresponding 2-amino-4*H*-chromene derivatives is suggested in Scheme 3. Likely, the initial step involves the condensation reaction between the aldehyde and malononitrile in the presence of Fe_3O_4@SiO_2-imine/phenoxy-Cu(II) as a Lewis acid catalyst to generate arylidenemalononitrile (**I**). In the following step, the resulted intermediate (**I**) undergoes a Michael-type addition reaction with the phenolic species (α-naphthol, β-naphthol, resorcinol or 2-hydroxynaphthalene-1,4-dione) under the catalytic acceleration to produce the adduct (**II**). Finally, enolization of (**II**) occur to yield the intermediate (**III**) which undergoes intramolecular nucleophilic cyclization to afford the respective products **7–10**.[71]

3.5 | Catalyst recyclability

We examined the recycling and reusability of the Fe_3O_4@SiO_2-imine/phenoxy-Cu(II) catalyst for the model reaction between benzaldehyde, malononitrile and α-naphthol under the optimized conditions. After completion of the reaction, the catalyst was separated magnetically using a magnet. The isolated nanoparticles were washed with ethanol and water several times, oven-dried at 60 °C, and reused for five successive runs with no significant loss of activity (Figure 8).

4 | THEORETICAL STUDIES

Theoretical calculations were performed to analyze the optimization of the molecular structures of 2-amino-4*H*-

chromene derivatives by using density functional theory (DFT)/B3LYP method. The most important geometrical parameters of the target compounds are quoted in Table 5. The frontier molecular orbitals, *i.e.* the highest occupied molecular orbital (HOMO) and the lowest unoccupied molecular orbital (LUMO), of 2-amino-4*H*-chromene derivatives are presented as Figure 1 in supplementary data. In addition, some considerable electronic features such as calculated bond lengths, dipole moments and energies of the HOMO and LUMO for all 2-amino-4*H*-chromene derivatives are listed in Table 5. As can be seen from this table, the higher negative charge density in the HOMO molecular orbitals, was found to be around the nitrogen atoms of the NH_2 and CN groups in 2-amino-4*H*-chromene derivatives. This observation implies the increased probability of nucleophilic attack of these groups at the metal ion. Moreover, the negative charge density of LUMO molecular orbitals has been nearly delocalized over the entire molecule. The higher energy of HOMO and the lower energy of LUMO facilitate the interaction between the electron-donor and electron-acceptor units.

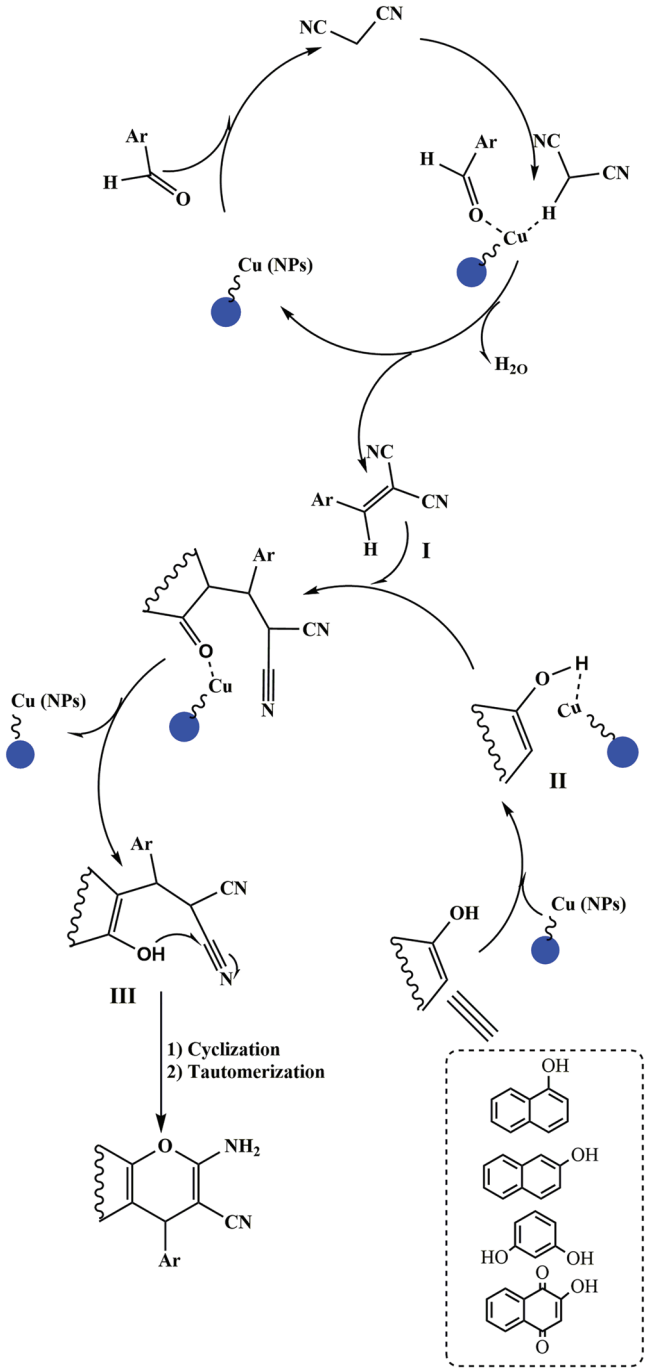

SCHEME 3 A plausible pathway for one-pot synthesis of 2-amino-4*H*-chromenes catalyzed by Fe_3O_4@SiO_2-imine/phenoxy-Cu (II) MNPs

5 | CONCLUSIONS

In the present research, we report for the first time the preparation of a new Cu(II) Schiff-base complex immobilized on silica-coated Fe_3O_4 magnetic nanoparticles. The prepared Fe_3O_4@SiO_2-imine/phenoxy-Cu(II) catalyst was structurally characterized by FT-IR, SEM, TEM, EDX, XRD, TGA, XPS, VSM and ICP-OES analytical techniques. These newly prepared nanoparticles were explored as efficient heterogeneous Lewis acid catalyst for the synthesis of various 2-amino-4*H*-chromene derivatives via one-pot three-component reactions between aldehydes, malononitrile and phenolic reagents such as α-naphthol, β-naphthol, resorcinol and 2-hydroxynaphthalene-1,4-dione under green solvent-free condition. Moreover, this catalyst can be easily recycled and reused for five times without significant loss of catalytic activity.

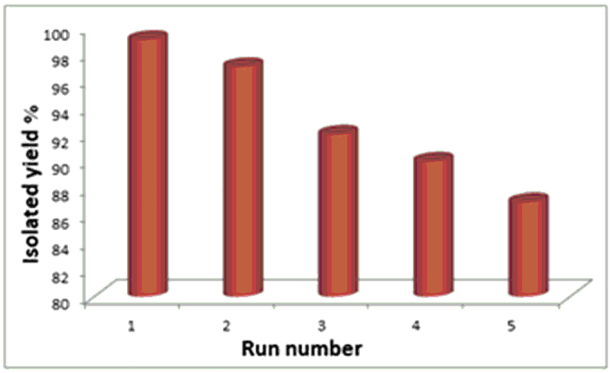

FIGURE 8 Recyclability of the Fe_3O_4@SiO_2-imine/phenoxy-Cu(II) catalyst

TABLE 5 Some theoretically computed HOMO, LUMO energies, dipole moments and selected structure parameters of DFT of 2-amino-4*H*-chromene derivatives

					Bond Length (Å)							
Samples	**E (HOMO)**	**E (LUMO)**	**ΔE (L-H)**	**dipole**	**O20-C13**	**N22-C21**	**C21-C13**	**C13-C12**	**C12-N23**	**C12-C11**	**C11-C26**	
7a	−0.19936	−0.04482	0.15454	5.2047	1.3859	1.1661	1.4209	1.358	1.379	1.5151	1.5346	
7b	−0.19758	−0.04975	0.14783	6.0287	1.3852	1.1661	1.4201	1.3567	1.379	1.515	1.5395	
7c	−0.21076	−0.0981	0.11266	6.1927	1.3834	1.1656	1.422	1.3575	1.381	1.5147	1.5346	
7d	−0.19743	−0.04225	0.15518	5.4891	1.3864	1.1662	1.4208	1.3581	1.3789	1.5152	1.5333	
7e	−0.19803	−0.04321	0.15482	6.1486	1.3861	1.1661	1.4209	1.358	1.379	1.5156	1.5331	
					O20-C11	N22-C21	C21-C11	C11-C12	C12-N23	C12-C13	C13-C26	
8a	−0.20119	−0.0441	0.15709	5.2743	1.3872	1.1665	1.4187	1.3589	1.3723	1.5172	1.5376	
8b	−0.20704	−0.05116	0.15588	5.0234	1.3813	1.1658	1.4215	1.3553	1.3824	1.5171	1.5421	
					N18-C17	C17-C11	C11-C12	C12-N14	C12-O13	O13-C3	C1-O19	
9a	−0.2106	−0.02248	0.18812	4.8123	1.1678	1.4174	1.3653	1.3662	1.356	1.3877	1.3643	
9b	−0.22178	−0.08781	0.13397	8.0625	1.1677	1.4173	1.3672	1.3626	1.355	1.3878	1.3626	
9c	−0.21793	−0.03418	0.18375	5.6778	1.1677	1.4173	1.3668	1.3633	1.3551	1.3887	1.3633	
9d	−0.21256	−0.02374	0.18882	4.6666	1.1677	1.4173	1.3662	1.3653	1.355	1.3871	1.3639	
9e	−0.21614	−0.02973	0.18641	5.4991	1.1678	1.4174	1.3667	1.3639	1.3551	1.3887	1.3636	
9f	−0.22357	−0.02148	0.20209	4.7831	1.1831	1.4178	1.3649	1.3669	1.3564	1.3876	1.3645	
					N22-C21	C21-C11	C11-C12	C12-N18	C12-O17	O17-C7	C34-O35	C36-O37
10a	−0.22494	−0.12086	0.10408	4.849	1.1674	1.4174	1.3637	1.362	1.3675	1.3665	1.2217	1.2263
10b	−0.23762	−0.13128	0.10634	8.1777	1.1672	1.4173	1.3649	1.3592	1.3674	1.3654	1.2211	1.2268
10c	−0.22619	−0.12401	0.10218	4.9973	1.1675	1.4164	1.3642	1.3582	1.3657	1.3625	1.221	1.227
10d	−0.23536	−0.13165	0.10371	6.7442	1.1672	1.4171	1.3657	1.3564	1.3674	1.3645	1.2208	1.2274
10e	−0.21864	−0.12159	0.09705	5.0934	1.1674	1.4167	1.3639	1.3617	1.3665	1.3649	1.2217	1.2255
10f	−0.28471	−0.23259	0.05212	4.5114	1.1676	1.4173	1.3636	1.3639	1.3668	1.3675	1.2224	1.2265
10 g	−0.22311	−0.11987	0.10324	4.6796	1.1674	1.4175	1.3635	1.3625	1.3673	1.3665	1.2219	1.2264

ACKNOWLEDGMENTS

The authors wish to thank the Research Council of Bu-Ali Sina University for financial support to carry out this research.

ORCID

Hakimeh Ebrahimiasl https://orcid.org/0000-0001-6690-5820

Davood Azarifar https://orcid.org/0000-0002-7331-2748

REFERENCES

[1] A. Loupy, *C. R. Chim.* **2004**, *7*, 103.

[2] (a) P. T. Anastas, T. Williamson, *Green Chemistry: Frontiers in Benign Chemical Synthesis and Process*, Oxford University Press, Oxford **1998**. (b) S. Rostamnia, K. Lamei, *Synthesis* 2011, *11*, 3080. (c) E. Doustkhah, S. Rostamnia, *J. Mol. Cat. A* 2016, *411*, 317. (d) Y. Zhang, X. Yang, Y. Zhou, G. Li, Z. Li, C. Liu, M. Bao, W. Shen, *Nanoscale* 2016, *8*, 18626. (e) G. H. Liu, K. X. Chen, H. P. Zhou, K. G. Ren, C. Pereira, J. M. F. Ferreira, *Key Eng. Mater.* 2007, *336*, 930. (f) A. Alizadeh, Q. Oskueyan, S. Rostamnia, *Synthesis* 2007, *17*, 2637. (g) A. Alizadeh, S. Rostamnia, A. A. Esmaili, *Synthesis* 2007, 709. (h) S. Rostamnia, E. Doustkhah, A. Nuri, *J. Fluorine Chem.* 2013, *153*, 1. (i) S. Rostamnia, *RSC Adv.* 2015, *5*, 97044.

[3] R. B. Nasir Baig, R. S. Varma, *Green Chem.* **2013**, *15*, 1839.

[4] D. D. Someshwar, G. P. Vedavati, T. J. Yeon, *Tetrahedron Lett.* **2012**, *53*, 4376.

[5] P. G. Rambhau, P. R. A. Ambarsing, *Drug Invention Today* **2013**, *5*, 148.

[6] (a)L. Yunyun, Z. Rihui, W. Jie-Ping, *Synth. Commun.* **2013**, *43*, 2475. (b) S. Sajjadifar, Z. Arzehgar, S. Khoshpoori, *J. Inorg. Organomet. P.* 2018, *28*, 837. (c) S. Sajjadifar, S. Rezayati, Z. Arzehgar, S. Abbaspour, M. Torabi Jafroudi, *J. Chin. Chem. Soc.* 2018, *65*, 960.

[7] X. Wu, C. Lu, Z. Zhou, G. Yuan, R. Xiong, X. Zhang, *Environ. Sci. Nano* **2014**, *1*, 71.

[8] (a) R. J. Yolanda de Miguel, *Chem. Soc. Perkin Trans* **2000**, *1*, 4213. (b) U. Shaikh, Q. Tamboli, S. Pathange, Z. Dahan, Z. Pudukulathan, *Chem. Methodol.* 2018, *2*, 73. (c) I. Sheikhshoaie, Z. Tohidiyan, *Chem. Methodol.* 2019, *3*, 30. (d) S. Taghavi Fardood, A. Ramazani, F. Moradnia, Z. Afshari, S. Ganjkhanlu, F. Yekke Zare, *Chem. Methodol.* 2019, *3*, 696.

[9] R. A. Sheldon, H. Van Bekkum, *Fine Chemicals through Heterogeneous Catalysis*, Wiley-VCH, Weinheim **2001**.

[10] (a) C. O. Dalaigh, S. A. Corr, Y. G. Ko, S. J. Connon, *Angew. Chem. Int. Ed.* **2007**, *46*, 4329. (b) I. Sheikhshoaie, S. Davary, S. Ramezanpour, *Methodol.* 2018, *2*, 47. (c) Z. Arzehgar, V. Azizkhani, S. Sajjadifar, M. Fekri, *Chem. Methodol.* 2019, *3*, 251. (d) R. Mohammadi, A. Sajjadi, *J. Med. Chem. Sci.* 2019, *2*, 55. (e) S. Taghavi Fardood, A. Ramazani, P. Azimzadeh Asiabi, Y. Bigdeli Fard, B. Ebadzadeha, *Asian J. Green Chem.* 2017, *1*, 34.

[11] (a) F. Shi, M. K. Tse, M. M. Pohl, A. Bruckner, S. Zhang, M. Beller, *Angew. Chem. Int. Ed.* **2007**, *46*, 8866. (b) S. Taghavi Fardood, A. Ramazani, M. Ayubi, F. Moradnia, S. Abdpour, R. Forootan, *Chem. Methodol.* 2019, *3*, 583. (c) S. Rezayati, Z. Abbasi, E. Rezaee Nezhad, R. Hajinasir, A. Farrokhnia, *Res. Chem. Intermed.* 2016, *42*, 7597. (d)S. Sajjadifar, S. Rezayati, A. Shahriari, S. Abbaspour, *Appl. Organomet. Chem.* 2018, *32*, e4172.

[12] J. H. Clark, D. J. Macquarrie, *Green Chemistry and Technology*, Blackwell, Abingdon **2002**.

[13] X. Zheng, S. Luo, L. Zhang, J.-P. Cheng, *Green Chem.* **2009**, *11*, 455.

[14] (a) M. Sorbiun, E. Shayegan Mehr, A. Ramazani, S. Taghavi Fardood, *J. Mater. Sci.: Mater. Electron.* **2018**, *29*, 2806. (b) S. Rostamnia, E. Doustkhah, *J. Magn. Magn. Mater.* 2015, *386*, 111. (c) S. Rostamnia, B. Zeynizadeh, E. Doustkhah, A. Baghban, K. O. Aghbash, *Catal. Commun.* 2015, *68*, 77.

[15] A. Azarifar, R. Nejat-Yami, M. Al Kobaisi, D. Azarifar, *J. Iran. Chem. Soc.* **2013**, *10*, 439.

[16] J. Govan, Y. K. Gun'ko, *Nanomaterials* **2014**, *4*, 222.

[17] L. L. Chng, N. Erathodiyil, J. Y. Ying, *Acc. Chem. Res.* **2013**, *46*, 1825.

[18] R. N. Baig, R. S. Varma, *Chem. Commun.* **2013**, *49*, 752.

[19] S. Shylesh, V. Schünemann, W. R. Thiel, *Angew. Chem. Int. Ed.* **2010**, *49*, 3428.

[20] A. Ghorbani-Choghamarani, B. Tahmasbi, N. Noori, S. Faryadi, *C. R. Chim.* **2017**, *20*, 132.

[21] Y. Zhu, L. P. Stubbs, F. Ho, R. Liu, C. P. Ship, J. A. Maguire, N. S. Hosmane, *ChemCatChem* **2010**, *2*, 365.

[22] A. Ghorbani-Choghamarani, B. Tahmasbi, Z. Moradi, *Appl. Organomet. Chem.* **2017**, *31*, e3665.

[23] C. W. Lim, I. S. Lee, *Nano Today* **2010**, *5*, 412.

[24] D. Wang, D. Astruc, *Chem. Rev.* **2014**, *114*, 6949.

[25] L. Shiri, B. Tahmasbi, *Sulfur Silicon* **2017**, *192*, 53.

[26] P. G. Cozzi, *Chem. Soc. Rev.* **2004**, *33*, 410.

[27] J. M. Khurana, B. Nand, P. Saluja, *Tetrahedron* **2010**, *66*, 5637.

[28] J. Bloxham, C. P. Dell, C. W. Smith, *ChemInform* **1994**, 25.

[29] A. Q. Zhang, M. Zhang, H. H. Chen, J. Chen, H. Y. Chen, *Synth. Commun.* **2007**, *37*, 231.

[30] J. Goujon, F. Zammattio, S. Pagnoncelli, Y. Boursereau, B. Kirschleger, *Synlett* **2002**, 0322.

[31] S. Khaksar, A. Rouhollahpour, S. M. Talesh, *J. Fluorine Chem.* **2012**, *141*, 11.

[32] M. A. Panchbhai, L. J. Paliwal, N. S. Bhave, *E- J. Chem.* **2008**, *5*, 1048.

[33] P. M. Reddy, K. Shanker, R. Rohini, V. Ravinder, *Int. J. ChemTech Res.* **2009**, *1*, 367.

[34] V. Alexander, *Chem. Rev.* **1995**, *95*, 273.

[35] S. Chandra, A. Gautum, M. Tyagi, *Trans. Met. Chem.* **2007**, *32*, 1079.

[36] D. P. Singh, K. Kumar, S. S. Dhiman, J. Sharma, J. Enzyme, *Inhib. Med. Chem.* **2010**, *25*, 21.

[37] M. Kidwai, N. K. Mishra, S. Bhardwaj, A. Jahan, A. Kumar, S. Mozumdar, *ChemCatChem* **2010**, *2*, 1312.

[38] L. Ding, A. Tselev, J. Wang, D. Yuan, H. Chu, T. P. McNicholas, Y. Li, J. Liu, *Nano Lett.* **2009**, *9*, 800.

[39] N. N. Hoover, B. J. Auten, B. D. Chandler, *J. Phys. Chem.* **2006**, *110*, 8606.

[40] R. Motamedi, G. Rezanejade Bardajee, S. Makenali Rad, *Asian J. Green Chem.* **2017**, *1*, 89.

[41] H. Aghahosseini, A. Ramazani, K. Ślepokura, T. Lis, *J. Colloid Interface Sci.* **2018**, *511*, 222.

[42] A. Ramazani, A. Tofangchi Mahyari, M. Rouhani, A. Rezaei, *Tetrahedron Lett.* **2009**, *50*, 5625.

[43] S. Rostamnia, E. Doustkhah, *RSC Adv.* **2014**, *4*, 23238.

[44] S. Rostamnia, E. Doustkhah, *Synlett* **2015**, *26*, 1345.

[45] S. Rostamnia, E. Doustkhah, *Tetrahedron Lett.* **2014**, *55*, 2508.
[46] C. O. Chichester, *The chemistry of plant pigments*, Academic Press, NY **1972**.
[47] S. Gao, C. H. Tsai, C. Tseng, C. F. Yao, *Tetrahedron* **2008**, *64*, 9143.
[48] D. Kumar, V. B. Sharad, S. U. Dube, S. Kapur, *J. Eur. Med. Chem.* **2009**, *44*, 3805.
[49] A. Tanabe, H. Nakashima, O. Yoshida, N. Yamamoto, O. Tenmyo, T. Oki, *J. Antibiot.* **1988**, *41*, 1708.
[50] A. Bolognese, G. Correale, M. Manfra, A. Lavecchia, O. Mazzoni, E. Novellino, P. La Colla, G. Sanna, R. Loddo, *J. Med. Chem.* **2004**, *47*, 849.
[51] J. A. Joule, K. Mills, G. F. Smith, *Heterocyclic Chemistry*, 3rd ed., Chapman & Hall, London **1995** 166.
[52] N. Morita, M. Arisawa, *Heterocycles* **1976**, *4*, 373.
[53] H. Schmid, *Chem. Org. Naturst.* **1954**, *11*, 124.
[54] Y. Peng, G. Song, *Catal. Commun.* **2007**, *8*, 111.
[55] T.-S. Jin, L.-B. Liu, Y. Zhao, T.-S. Li, *Synth. Commun.* **2005**, *35*, 1859.
[56] S. Balalaie, S. Abdolmohammadi, *Tetrahedron Lett.* **2007**, *48*, 3299.
[57] B. N. Seshu, N. Pasha, R. K. T. Venkateswara, P. P. S. Sai, N. Lingaiah, *Tetrahedron Lett.* **2008**, *49*, 2730.
[58] H. Nagabhushana, S. S. Saundalkar, L. Muralidhar, B. M. Nagab-hushana, C. R. Girija, D. Nagaraja, M. A. Pasha, V. P. Jayashankara, *Chin. Chem. Lett.* **2011**, *22*, 143.
[59] K. Niknam, A. Piran, *Green Sustain. Chem.* **2013**, *3*, 1.
[60] M. M. Heravi, B. Alimadadi Jani, F. Derikvand, F. F. Bamoharram, H. A. Oskooie, *Catal. Commun.* **2008**, *10*, 272.
[61] A. D. Becke, *J. Chem. Phys.* **1993**, *98*, 5648.
[62] M. B. Gawande, A. K. Rathi, P. S. Branco, I. D. Nogueira, A. Velhinho, J. J. Shrikhande, U. U. Indulkar, R. V. Jayaram, C. A. A. Ghumman, N. Bundaleski, *Chem. – Eur. J.* **2012**, *18*, 12628.
[63] E. D. Glendening, J. Badenhoop, F. Weinhold, *J. Comput. Chem.* **1998**, *19*, 628.
[64] C. Lee, W. Yang, R. G. Parr, *Phys. Rev. B* **1988**, *37*, 785.
[65] M. Ma, Y. Zhang, X. Li, D. Fu, H. Zhang, N. Gu, *Colloids Surf., a* **2003**, *224*, 207.
[66] M. Tajbakhsh, M. Farhang, R. Hosseinzadeh, Y. Sarrafi, *RSC Adv.* **2014**, *4*, 23116.
[67] H. Cao, J. He, L. Deng, X. Gao, *Appl. Surf. Sci.* **2009**, *255*, 7974.
[68] H. Zhu, Y. Hu, G. Jiang, G. Shen, *Eur. Food Res. Technol.* **2011**, *233*, 881.
[69] H. Keypour, M. Mahmoudabadi, A. Shooshtari, M. Bayat, F. Mohsenzadeh, R. William Gable, *J. Mol. Struct.* **2018**, *1155*, 196.
[70] M. Ghorbanloo, R. Bikas, G. Małecki, *Inorg. Chim. Acta* **2016**, *445*, 8.
[71] J. Safari, Z. Zarnegar, M. Heydarian, *Bull. Chem. Soc. Jpn.* **2012**, *85*, 1332.
[72] D. Chen, S. Huang, *J. Micro Nanolithogr. MEMS MOEMS* **2016**, *15*, 035005.
[73] X. Fu, X. Hu, Z. Yan, K. Lei, F. Li, F. Cheng, J. Chen, *Chem. Commun.* **2016**, *52*, 1725.
[74] M. Gholinejad, F. Zareh, C. Najera, *Appl. Organomet. Chem.* **2018**, *32*, e4454.
[75] M. Gholinejad, E. Oftadeh, J. M. Sansano, *ChemistrySelect* **2019**, *4*, 3151.
[76] S. Paul, P. Bhattacharyya, A. R. Das, *Tetrahedron Lett.* **2011**, *52*, 4636.
[77] B. S. Kumar, N. Srinivasulu, R. Udupi, B. Rajitha, Y. T. Reddy, P. N. Reddy, P. Kumar, *Russ. J. Org. Chem.* **2006**, *42*, 1813.
[78] D. S. Raghuvanshi, K. N. Singh, *ARKIVOC* **2010**, *10*, 305.
[79] H. R. Shaterian, M. Mohammadnia, *J. Mol. Liq.* **2013**, *177*, 353.
[80] A. Shaabani, R. Ghadari, S. Ghasemi, M. Pedarpour, A. H. Rezayan, A. Sarvary, S. W. Ng, *J. Comb. Chem.* **2009**, *11*, 956.
[81] J. B. Harborne, T. J. Mabry, *The flavonoids: Advances in research science 1980*, Chapman & Hall, London & NY **1988**.
[82] G. A. Iacobucci, J. E. Sweeny, *Tetrahedron* **1983**, *39*, 3005.
[83] A. Azarifar, R. Nejat-Yami, M. AlKobaisi, D. Azarifar, *J. Iran. Chem. Soc.* **2012**, *10*, 439.
[84] A. Azarifar, R. Nejat-Yami, D. Azarifar, *J. Iran. Chem. Soc.* **2013**, *10*, 297.
[85] D. Azarifar, Y. Abbasi, *Synth. Commun.* **2016**, *46*, 745.
[86] D. Azarifar, O. Badalkhani, Y. Abbasi, M. Hasanabadi, *J. Iran. Chem. Soc.* **2017**, *1*, 403.
[87] D. Azarifar, H. Ebrahimiasl, R. Karamian, M. Ahmadi-Khoei, *J. Iran. Chem. Soc.* **2019**, *16*, 341.
[88] D. Azarifar, M. Tadayoni, M. Ghaemi, *Appl. Organomet. Chem.* **2018**, *32*, e4293.
[89] D. Azarifar, S. Mahmoudi-GomYek, M. Ghaemi, *Appl. Organomet. Chem.* **2018**, *32*, e4541.
[90] S. Mahmoudi-GomYek, D. Azarifar, M. Ghaemi, H. Keypour, M. Mahmoudabadi, *Appl. Organomet. Chem.* **2019**, *33*, e4918.
[91] D. Azarifar, M. Ghaemi, R. Karamian, Y. Abbasi, F. Ghasemloub, M. Asadbegy, *New J. Chem.* **2018**, *42*, 1796.

SUPPORTING INFORMATION

Additional supporting information may be found online in the Supporting Information section at the end of this article.

How to cite this article: Ebrahimiasl H, Azarifar D. Copper-based Schiff Base Complex Immobilized on Core-shell Fe_3O_4@SiO_2 as a magnetically recyclable and highly efficient nanocatalyst for green synthesis of 2-amino-4*H*-chromene derivatives. *Appl Organometal Chem*. 2019;e5359. https://doi.org/10.1002/aoc.5359